Supplementary Information

A universal molecular mechanism driving aging

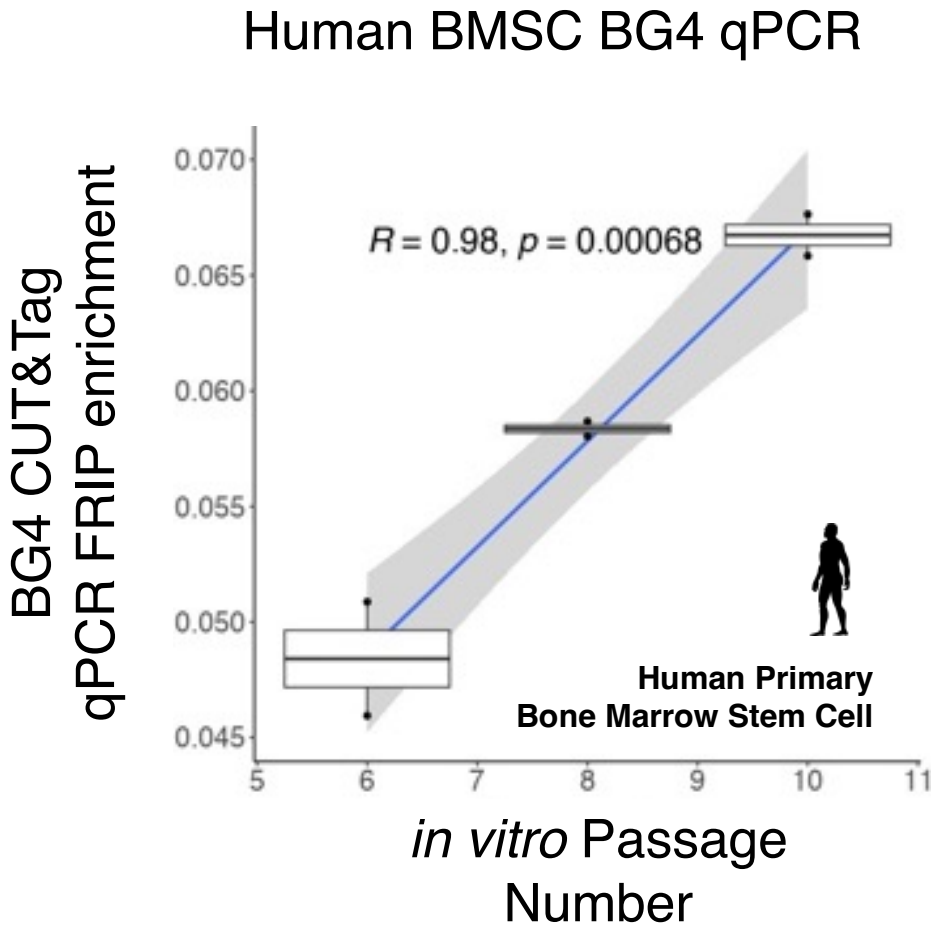

Extended Data Figure 1. G4 qPCR enrichment against library content for human BMSCs. qPCR amplification results with the G4 primer and Illumina P7 primer from the BG4 CUT&Tag libraries of hBMSCs are shown.

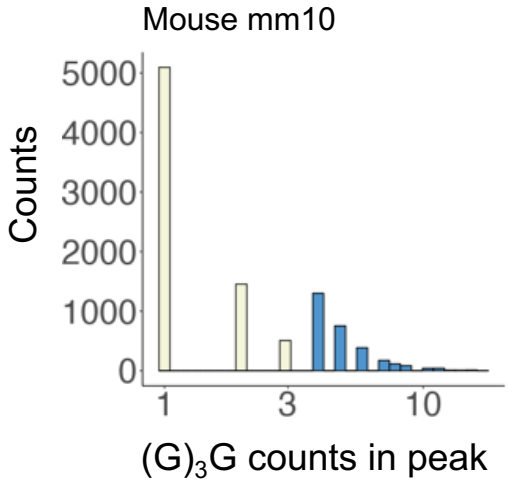

Extended Data Figure 2. Distribution of G3/G counts in each mouse ATAC peak. The blue columns are the peaks with >3 G3/G repeats.

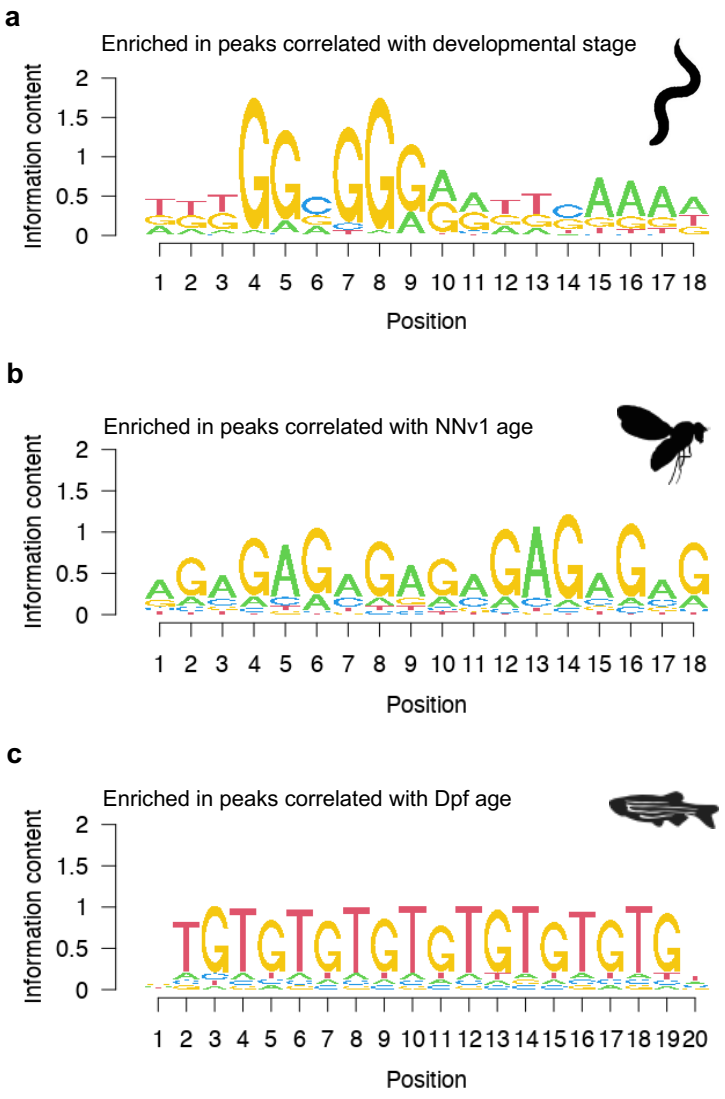

Extended Data Figure 3. Top enriched motif associated with age-associated chromatin opening.

(a) Top enriched motif in the *C. elegans* development ATAC dataset. **(b)** Top enriched motif in the *D. melanogaster* embryonic development scATAC dataset. **(c)** Top enriched motif in the *D. rerio* neural crest development scATAC dataset.

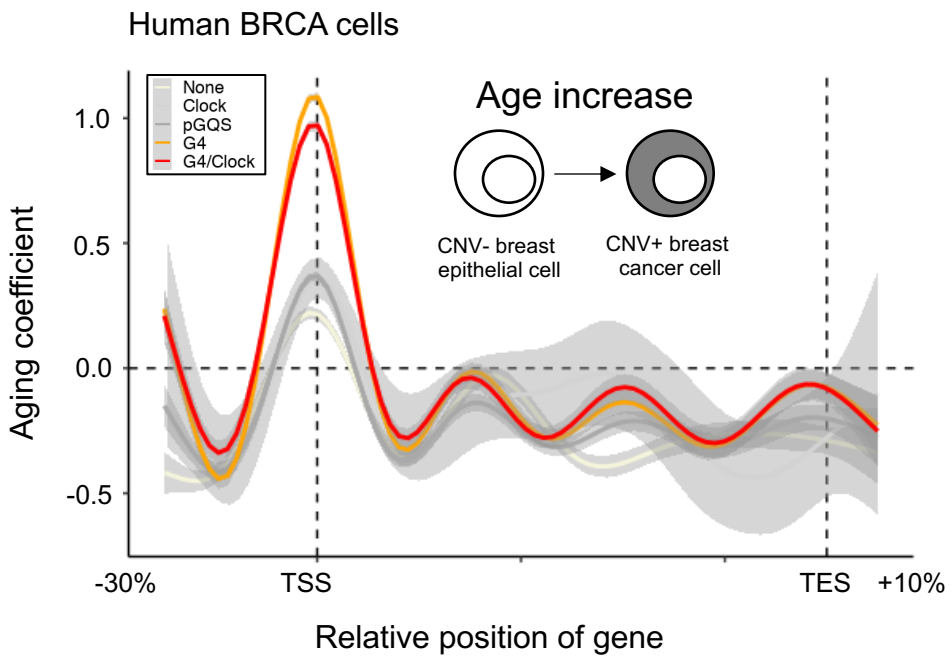

Extended Data Figure 4. Aging coefficient profiles of genes in human breast cancer cells. The genes were classified as (1) harboring ClockDML in the TSS; (2) harboring pGQS in the TSS; (3) harboring the G4-ChIP-seq signal in the TSS; (4) harboring both ClockDML and the G4-ChIP-signal; or (5) not harboring any of the above.

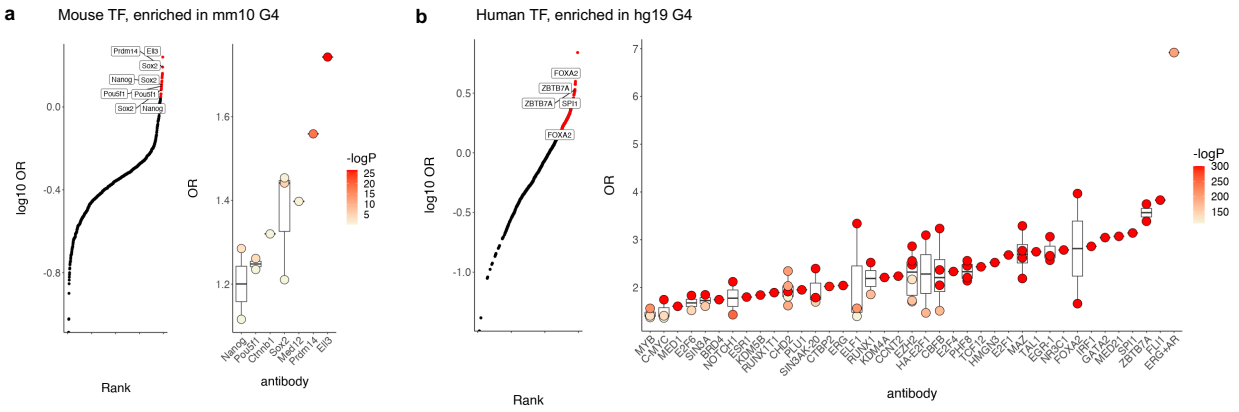

Extended Data Figure 5. Enrichment of TF-ChIP-seq peaks at pGQS loci in the mouse and human genomes.

(a) (left) Enrichment (Y-axis) vs rank (X-axis) of TF ChIP-seq peaks in pGQS in the mouse genome. The top 10% of enriched TFs are highlighted in red and labeled. (right) Enrichment (Y-axis) of the top enriched TFs. Individual ChIP-seq peak sets of the same TF are shown as dots and filled with log P-value denoting enrichment significance. **(b)** (left) Enrichment (Y-axis) vs rank (X-axis) of TF ChIP-seq peaks in pGQS in the human genome. The top 10% of enriched TFs are highlighted in red and labeled. (right) Enrichment (Y-axis) of the top enriched TFs. Individual ChIP-seq peak sets of the same TF are shown as dots and filled with log P-value denoting enrichment significance.

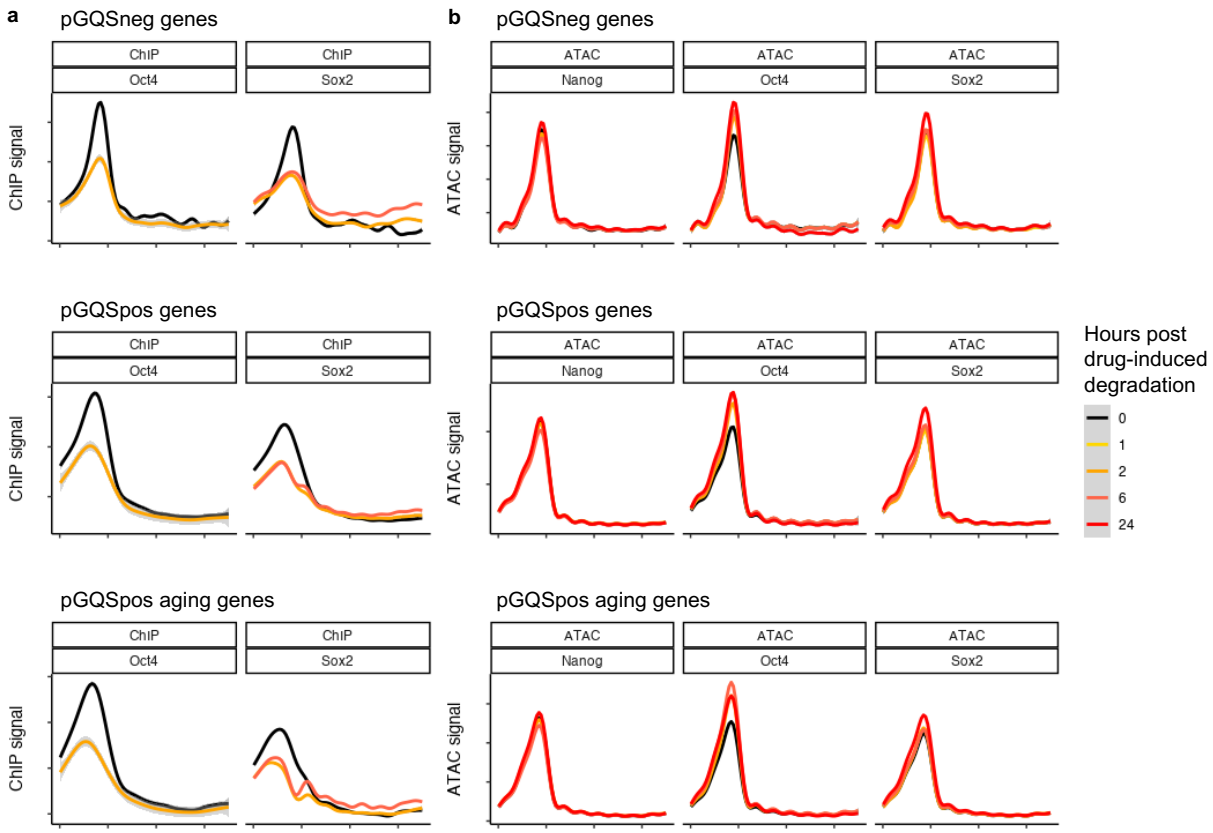

Extended Data Figure 6. Pioneering pluripotency factors that bind to pGQS but not regulate pGQS chromatin opening.

(a) ChIP-seq signal profiles of FKBP-Oct4 and FKBP-Nanog on the pGQSneg, pGQSpos, and pGQSpos aging genes. Drug-induced degradation of Oct4 and Nanog was performed for the indicated time length (denoted by color) for each sample. The control state is 0 hours. **(b)** ATAC-seq signal profiles of FKBP-Oct4, FKBP-Nanog and FKBP-Sox2 cells for the pGQSneg, pGQSpos, and pGQSpos aging genes. Drug-induced degradation of Oct4, Nanog and Sox2 was performed for the indicated time length (denoted by color) for each sample. The control state is 0 hours.

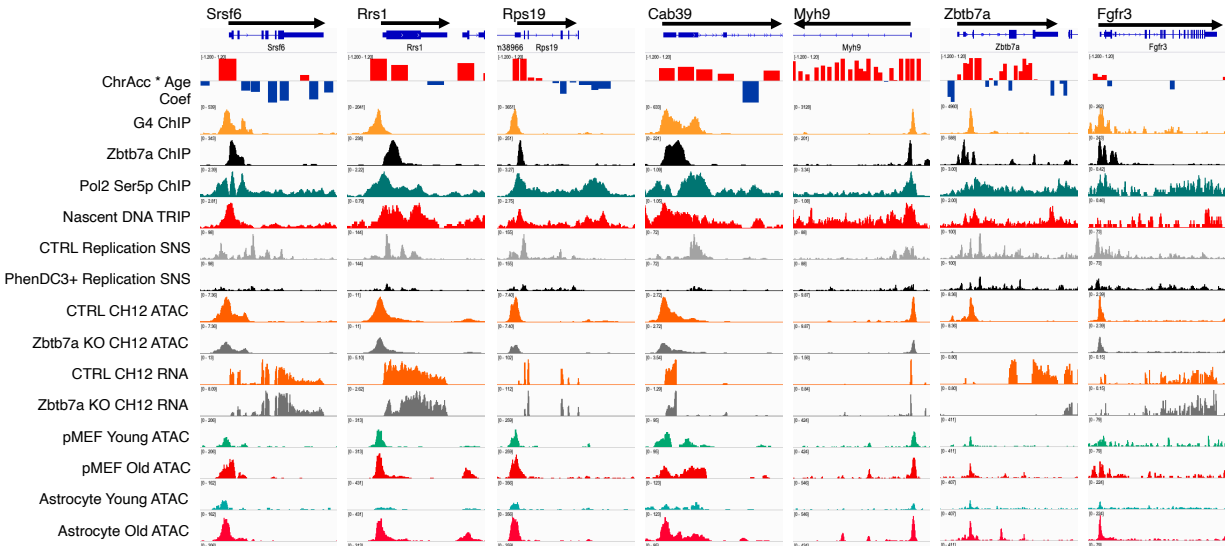

Extended Data Figure 7. Enrichment of G4, Zbtb7a binding, RNApol2 Ser5p, nascent DNA TRI, and G4-responsive DNA replication in aging genes in the mouse genome. The G4 ChIP-seq track was obtained from mESCs. The Zbtb ChIP-seq track was obtained from Ch12 cells. The pMEF and pAST ATAC results are also shown for comparison.

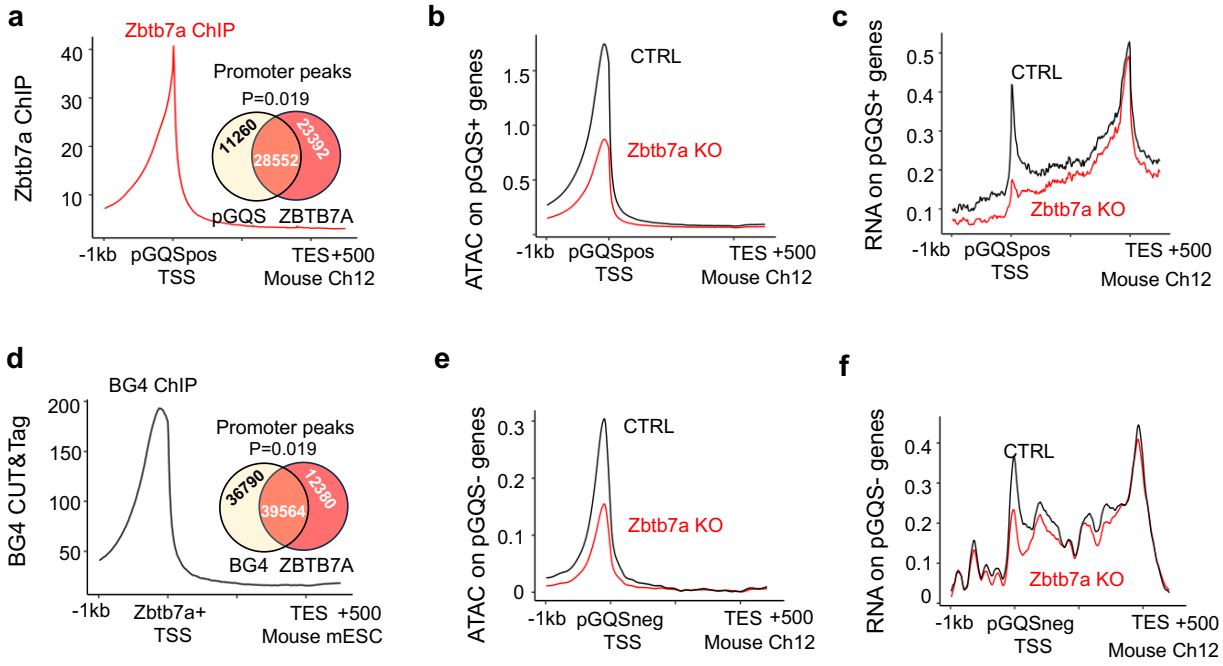

Extended Data Figure 8. Zbtb7a regulates G4 locus chromatin.

(a) ChIP-seq signal profiles of Zbtb7a on pGQSpos genes in mouse Ch12 cells. Inset: overlaps between Zbtb7a ChIP-seq peaks and pGQS loci (P=0.019 according to the permutation test). **(b)** ATAC-seq profiles of pGQSpos genes in control and Zbtb7a KO Ch12 cells. **(c)** RNA-seq profiles of pGQSpos genes in control and Zbtb7a KO Ch12 cells. **(d)** ChIP-seq signal profiles of G4s of the pGQSpos gene in mouse mESCs. Inset: overlaps between Zbtb7a and G4-ChIP-seq peaks (P=0.019 according to the permutation test). **(e)** ATAC-seq profiles of pGQSneg genes in control and Zbtb7a KO Ch12 cells. **(f)** RNAseq profiles of pGQSneg genes in control and Zbtb7a KO Ch12 cells.

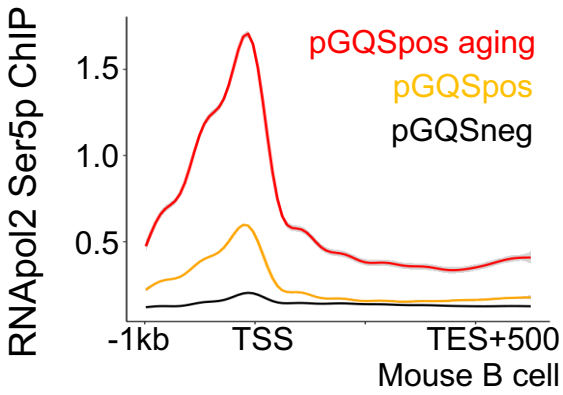

Extended Data Figure 9. RNApol2 Ser5p ChIP-seq profile of the pGQSneg, pGQSpos and pGQSpos aging genes in mouse B cells. Black: pGQSneg; orange: pGQSpos; and red: pGQSpos aging genes.

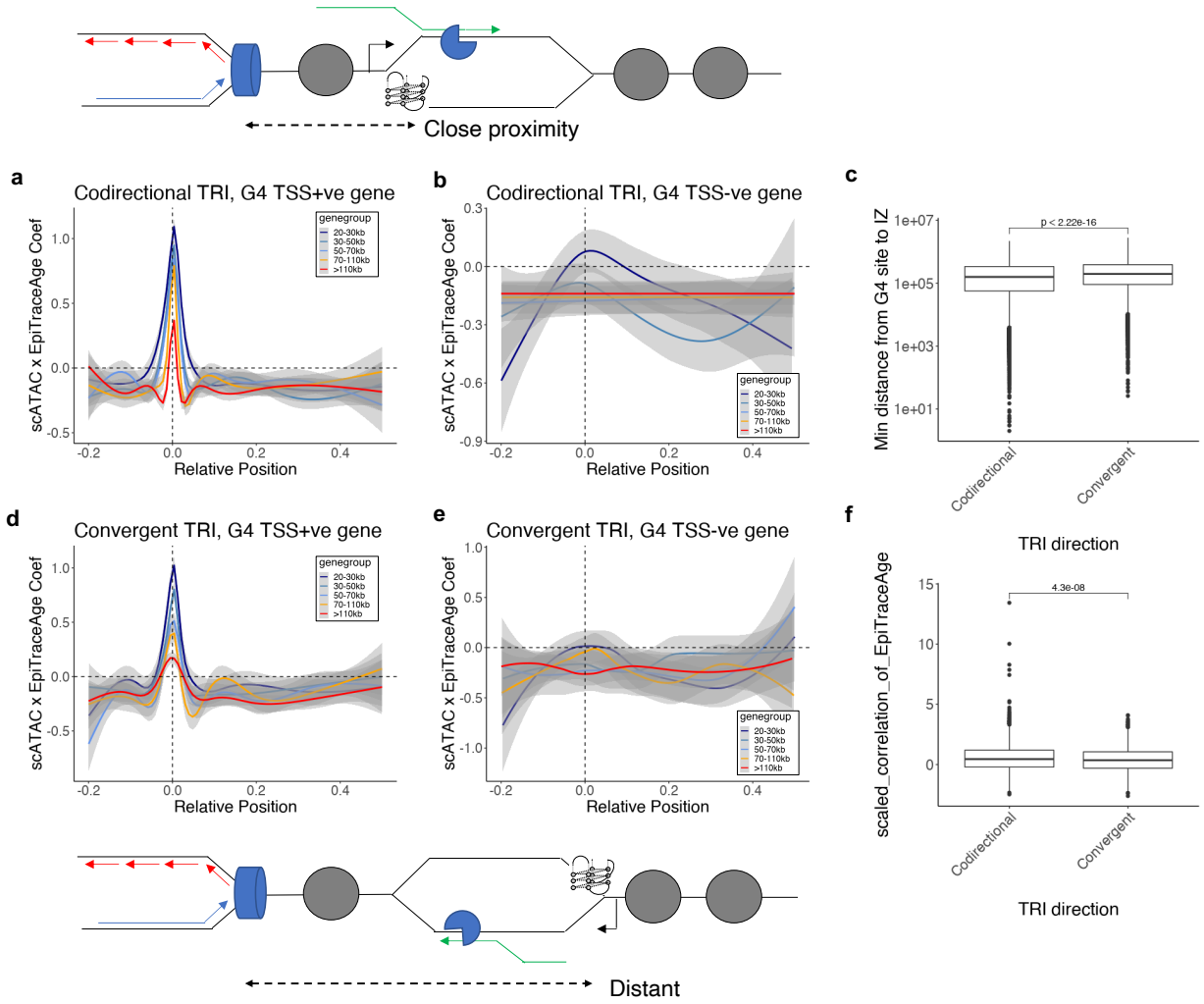

Extended Data Figure 10. TRI influences the aging coefficient of loci.

(a) Smoothened aging coefficient of pGQSpos genes with codirectional TRI. Genes were further classified according to their length. **(b)** Smoothened aging coefficient of pGQSneg genes with codirectional TRI. Genes were further classified according to their length. **(c)** Minimal distance between the pGQS locus and the replication initiation zone (IZ) in the codirectional or convergent TRI class of genes. **(d)** Smoothened aging coefficient of pGQSpos genes with convergent TRI. Genes were further classified according to their length. **(e)** Smoothened aging coefficient of

pGQSneg genes with convergent TRI. Genes were further classified according to their length. **(f)** Aging coefficient of pGQS loci in the codirectional or convergent-TRI class of genes.

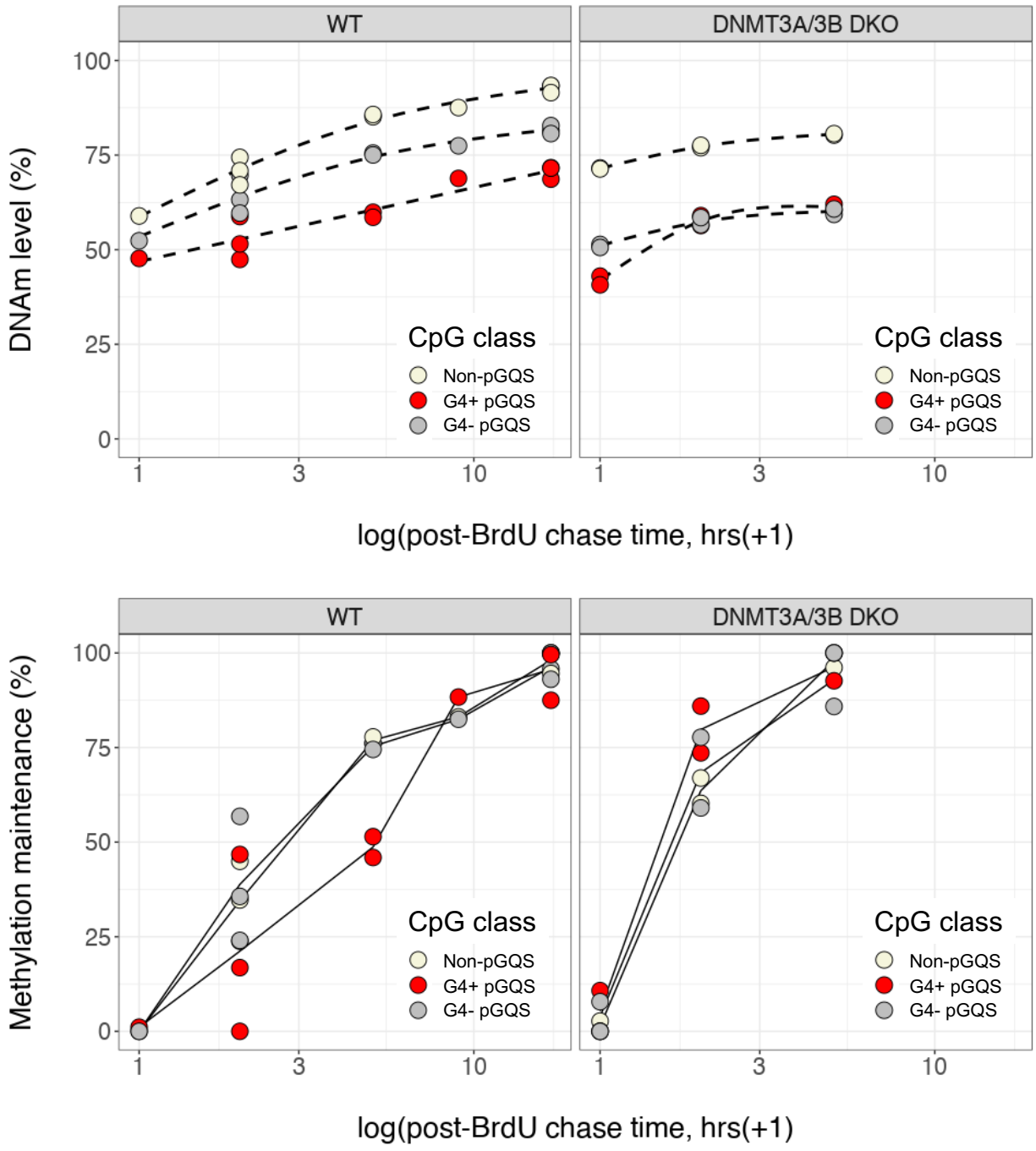

Extended Data Figure 11. G4 impairs DNA methylation maintenance in human embryonic stem cells.

(a) DNA methylation level (Y-axis) of each class of CpG in wild-type HUES64 cells pulsed with BrdU and chased with thymidine for the indicated times (X-axis). **(b)** DNA methylation level (Y-axis) of each class of CpG in DNMT3A/3B double knockout (DKO) HUES64 cells pulsed with BrdU and chased with thymidine for the indicated times (X-axis). **(c)** DNA methylation maintenance level (Y-axis), defined as the normalized (min-max) methylation level, of each class of CpG in wild-type HUES64 cells pulsed with BrdU and chased with thymidine for the indicated times (X-axis). **(b)** DNA methylation maintenance level (Y-axis) of each class of CpG in DNMT3A/3B DKO HUES64 cells pulsed with BrdU and chased with thymidine for the indicated times (X-axis).

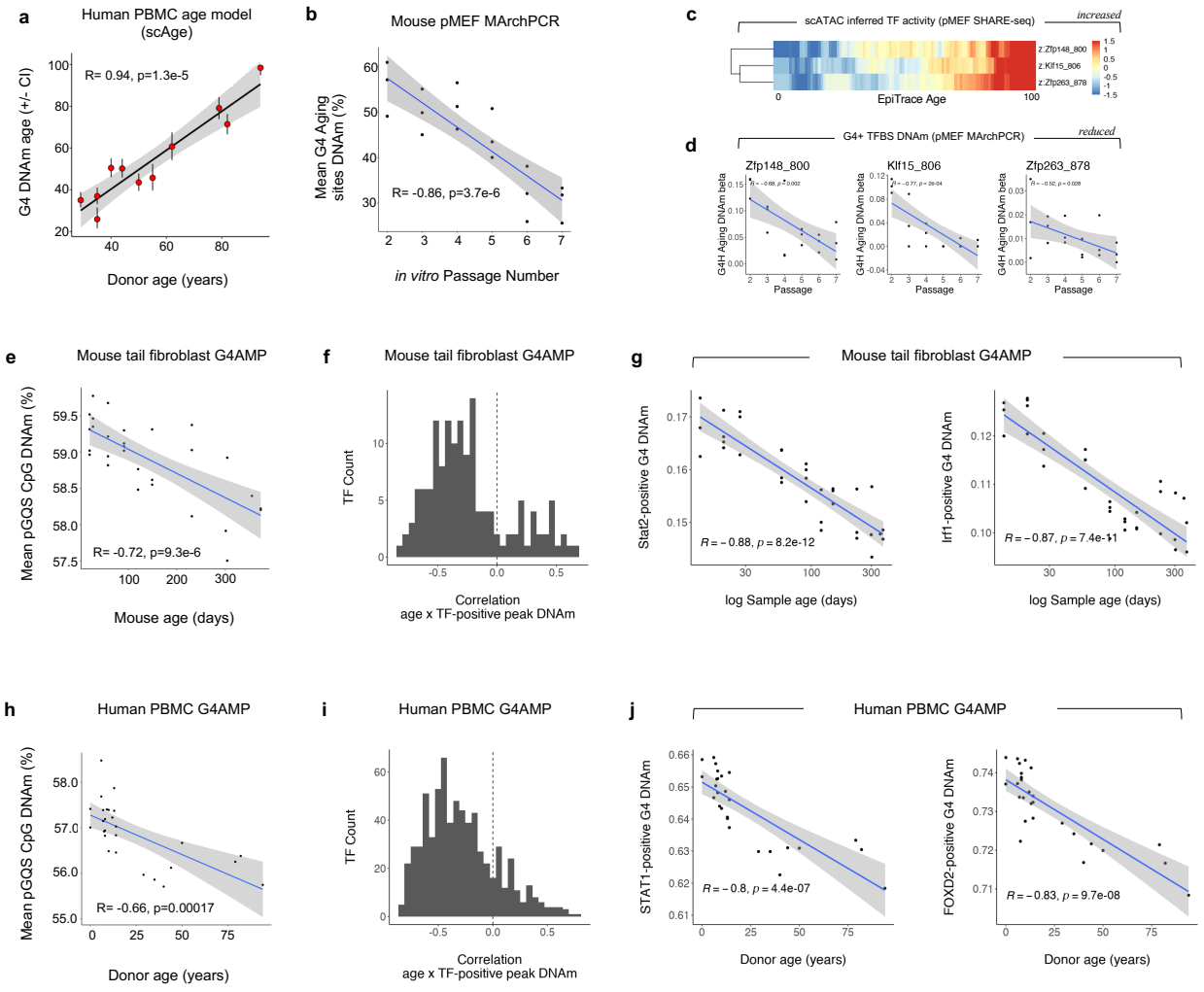

Extended Data Figure 12. G4 DNA hypomethylation *in vivo* during aging.

(a) Real (X-axis) and G4 DNAm-predicted age (scAge, Y-axis) of human PBMC samples sequenced by G4AMP. The 95% confidence intervals of the predicted biological age are also shown. **(b)** Mean DNA methylation level of age-associated CpGs in the vicinity of G4s in mouse pMEFs. **(c)** SHARE-seq scATAC data showing the transcription factor activities (color) of Zfp148, Zfp263, and Klf15 with respect to single-cell age (X-axis) in pMEFs. The inferred transcription factor activities are shown as Z-scaled normalized values. **(d)** Mean DNA methylation of G4 loci bound by Zfp148, Zfp263, and Klf15 in the same batch of pMEFs of different ages. **(e)** Mean DNA

methylation of G4 loci in primary mouse tail fibroblast samples of different ages. **(f)** The distribution of correlation coefficients between the mean DNA methylation level at the TF-bound G4 locus and sample age in the mouse tail fibroblast dataset. **(g)** Mean DNA methylation of Stat2-bound and Irf1-bound G4 loci in primary mouse tail fibroblast samples of different ages. **(h)** Mean DNA methylation of G4 loci in human PBMC samples of different ages from healthy donors. **(i)** The distribution of correlation coefficients between the mean DNA methylation level of TF-bound G4 loci and sample age in the human PBMC dataset. **(j)** Mean DNA methylation of the STAT1-bound and FOXD2-bound G4 loci in the human PBMC dataset.

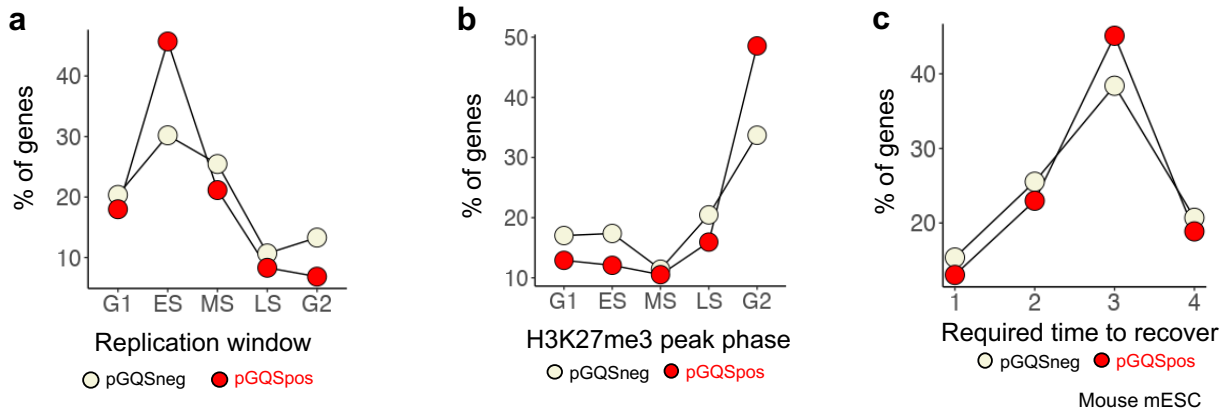

Extended Data Figure 13. H3K27me3 recovery during the cell cycle in the pGQSpos and pGQSneg genes in mouse mESCs.

(a) Percentage of genes that initiate replication (showing the lowest H3K27me3 signal) in the indicated cell cycle phase. **(b)** Percentage of genes that reached the maximal H3K27me3 signal in the indicated cell cycle phase. **(c)** Percentage of genes that required the indicated time (number of cell cycle phases, G1/ES/MS/LS/G2) to reach the maximal H3K27me3 value from the replication initiation phase.

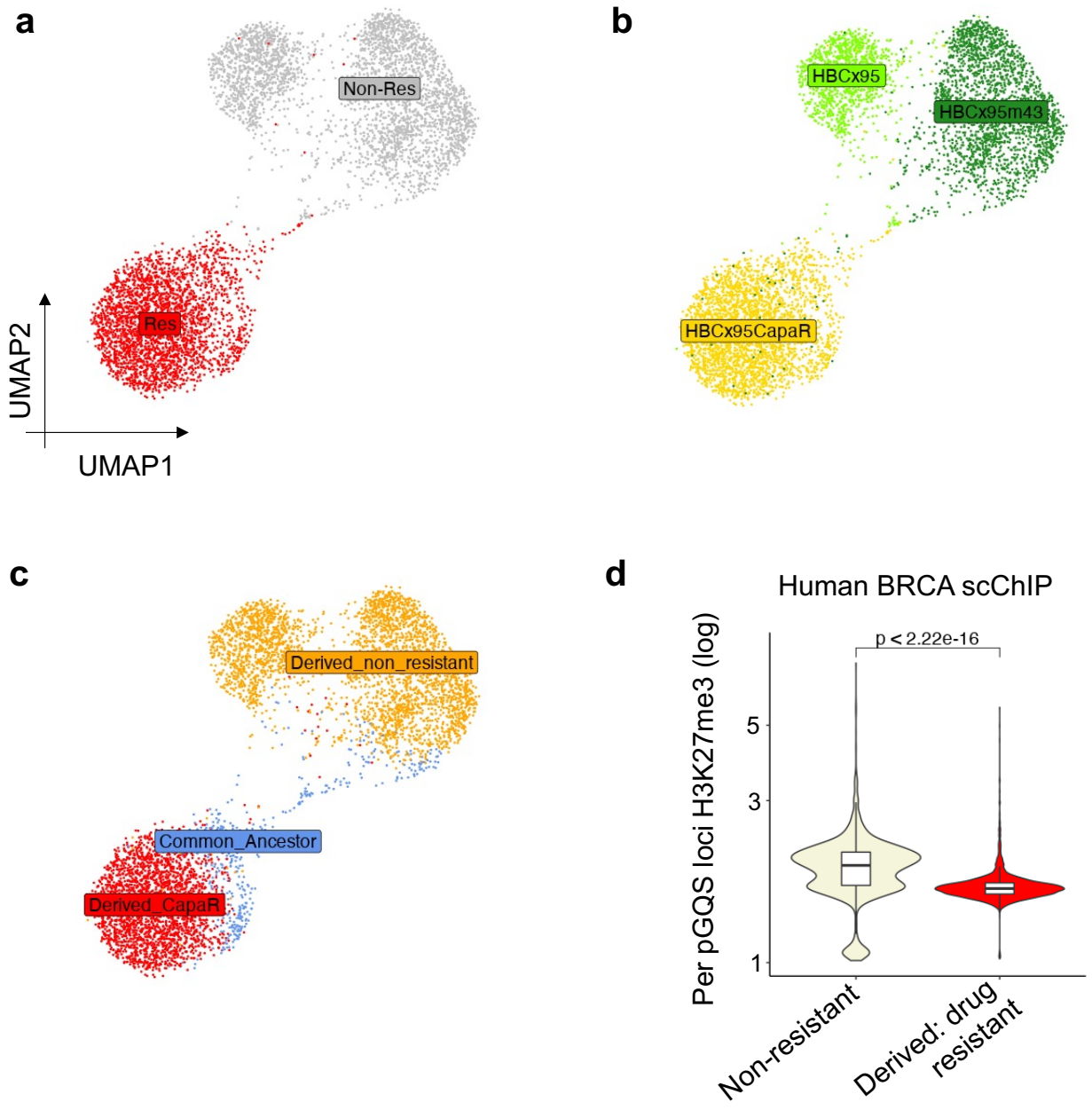

Extended Data Figure 14. H3K27me3 at the G4 locus is reduced during human BRCA cell aging

(a) UMAP plot of human BRCA cells from the scChIP-seq experiment, labeled by the capecitabine resistance state of each sample. **(b)** UMAP plot of human BRCA cells from the scChIP-seq

experiment, labeled by sample name. **(c)** UMAP projection of human BRCA cells from the scChIP-seq experiment, labeled by scChIP-seq profile-based single-cell clusters. **(d)** Mean H3K27me3 reads on each pGQS locus in the non-resistant or the derived drug-resistant cells, as in (a).

a

Patient	ID	Age	Mutation	Mutation class
P1	1902755	10	ERCC8 Exon 4 rearrangement / Exon 4 rearrangement	Hypomorph I
P2	1902750	8	ERCC8 Exon 4 rearrangement / c.394_398delTTACA	Hypomorph I
P3	1902752	7	ERCC8 Exon 4 rearrangement / IVS2+5delG	Hypomorph I
P4	1902751	6	ERCC8 Exon 4 rearrangement / Exon 4 rearrangement	Hypomorph I
P5	1902753	13	ERCC8 Exon 4 rearrangement / Deep intronic mutation	Hypomorph II
P6	1902749	14	ERCC8 Exon 4 rearrangement / Complex	Hypomorph II
P7	1902756	9	ERCC8 Exon 4 rearrangement / Large fragment deletion	Null

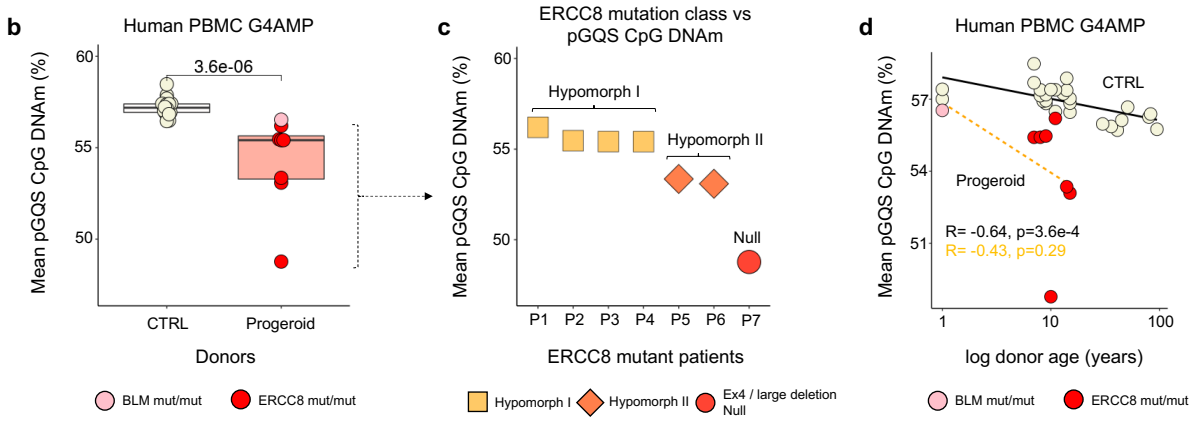

Extended Data Figure 15. Details of the progeroid patients.

(a) Genetic mutation details of each CSB patient. **(b)** Mean pGQS CpG DNAm of age-matched control (CTRL) or progeroid patients. **(c)** Mean pGQS CpG DNAm of ERCC8 mutant patients. **(d)** Relationship between age and the mean pGQS CpG DNAm in control or progeroid patients.

Extended Data Tables S1-S2

Extended Data Table 1. Public datasets used in this study.

Accession.Code / URL	Annotation
GSE131098	Hammerseq
GSE82045	Repli-BS-seq
https://github.com/CL-CHEN-Lab/OK-Seq	OK-seq
GSE165128	Ch12 cells (Zbtb7a KO ATAC-seq, Zbtb7a KO RNA-seq)
GSE209527	Sox2 Oct4 Nanog ChIP/ATAC
GSE178668	G4 ligand-treated TT-seq
GSE52285	WRN KO ChIP-seq
GSE161410	TRIPn-seq and RNAPol2 Ser5p ChIP-seq
GSE137764	High resolution Repli-seq
GSE126477	SNS-Seq
GSE118581	Yeast aging ATAC
GSE114494	C.elegans aging ATAC
GSE190149	Drosophila embryonic development scATAC
GSE178969	Zebrafish neural crest development scATAC
GSE74912	Human blood cell ATAC
GSE188461	Human chemically induced pluripotent stem cell scATAC
GSE198639	Human breast cancer scATAC
GSE152216	Human breast cancer G4 ChIP-seq
GSE173103	mESC G4 CUT&Tag
GSE187007	G4Access
GSE117309	Human breast cancer single-cell ChIP-seq (H3K27me3)
GSM803473	Human ZBTB7A ChIP-seq
GSE122937	Mouse Zbtb7a ChIP-seq
GSE209818	Mouse mESC H3K27me3 CUT&Flow

Extended Data Table S2. Patient information.

Patient	ID	Age	Mutation	Mutation class
ERCC8-P1	1902755	10	ERCC8 Exon 4 rearrangement / Exon 4 rearrangement	Hypomorph I
ERCC8-P2	1902750	8	ERCC8 Exon 4 rearrangement / c.394_398delTTACA	Hypomorph I
ERCC8-P3	1902752	7	ERCC8 Exon 4 rearrangement / IVS2+5delG	Hypomorph I
ERCC8-P4	1902751	6	ERCC8 Exon 4 rearrangement / Exon 4 rearrangement	Hypomorph I
ERCC8-P5	1902753	13	ERCC8 Exon 4 rearrangement / Deep intronic mutation	Hypomorph II
ERCC8-P6	1902749	14	ERCC8 Exon 4 rearrangement / Complex	Hypomorph II
ERCC8-P7	1902756	9	ERCC8 Exon 4 rearrangement / Large fragment deletion	Null
BLM-P1	2102456	0	BLM c.1544dup / c.3300A>G	PAT/LP